JOURNAL OF AIRCRAFT
Vol. 32, No. 5, September–October 1995

Wing Performance in Moderate Rain

B. E. Thompson,* J. Jang,† and J. L. Dion‡
Rensselaer Polytechnic Institute, Troy, New York 12180-3590

Emphasis is placed on the correlation of surface-film behavior including rivulet formulation with measured values of lift, drag, and moment at angles of attack up to stall. Four regions of surface flow are identified: 1) the droplet-impact, 2) film-convection, 3) rivulet-formation, and 4) droplet-convection regions. The extent that each of these regions covers the airfoil surface changes with incidence and correlates with changes in aerodynamic-force coefficients. Additionally, results quantify effects of the use of boundary-layer trips for linking flight and wind-tunnel models in rain, and show that surface water phenomena affect laminar-to-turbulent transition in a manner that is inconsistent with the use of transition fixing to increase the effective test Reynolds number.

Nomenclature

A_{wing} = wing planform area
C_d = drag coefficient, DRAG/qA_{wing}
C_l = lift coefficient, LIFT/qA_{wing}
C_m = moment coefficient, PITCHING MOMENT/qA_{wing}
c = chord length
Re = Reynolds number based on chord length and freestream velocity
α = angle of attack
ΔC_d = drag coefficient increment, $(C_d)_{wet} - (C_d)_{dry}$
$\Delta C_{l\%}$ = percent change in lift coefficient, $100 \times [(C_l)_{wet} - (C_l)_{dry}]/(C_l)_{dry}$
ΔC_m = moment coefficient increment, $(C_m)_{wet} - (C_m)_{dry}$

Introduction

WEATHER-RELATED factors contribute to more than 25% of the serious general aviation accidents annually in the U.S.[1] and this focuses attention on the aerodynamic performance of airfoils in rain. Heavy rain rates above about 1800 mm/h can decrease lift by up to 30% and increase drag by up to 20% (Ref. 2), affecting stall speed and the handling qualities of aircraft. In heavy rain, the airfoil surface near the leading edge is completely wetted and a sheet film forms and convects downstream.[3] Downstream at distances dependent on the Weber number, rivulets or water beads may form.[4] Rivulets significantly affect boundary-layer development either by reducing the Reynolds number at which transition occurs[5] or by increasing the surface roughness and skin friction,[6] or by changing the mechanism of laminar–turbulent transition. Transition can be influenced by film perturbations such as surface waves or turbulence in the surface film, rather than just from growth of instabilities from within the boundary-layer flow.

Even light-to-moderate rain rates effect increases in surface roughness and boundary-layer development due to the accumulation and behavior of surface water. The surface-water film may induce premature laminar-to-turbulent transition,[5] can result in early boundary-layer separation, and can cause aircraft to stall at higher indicated airspeeds than normal.[3] Stall–spin during the turn to final approach for landing is known by general-aviation pilots to be a cause of fatal accidents. High bank angles and a cross-controlled rudder can effect one wing to stall and the aircraft to spin, and this can happen during a landing approach with insufficient altitude to recover before impact. Rain increases the stall speed of aircraft and thus reduces the bank angle necessary for spin entry, and so it is for safety considerations in sport and general-aviation flying that this contribution quantifies rain effects at light and moderate rain rates.

The principal objective of this article is to understand the effects of rain on the performance of wings at low Reynolds number. Results are obtained at a low Reynolds number of 2.5×10^5, in part to provide insights useful in the design of natural laminar-flow airfoils,[3] which are anticipated for the next generation of general-aviation aircraft. Emphasis is placed on the combination of a low Reynolds number and light-to-moderate rain rates because low-Reynolds-number airfoils,[5] are affected by these low rain rates, in contrast to the commercial-aircraft wings of the heavy-rain studies discussed previously, because the lift, drag, and moment coefficients of laminar-flow airfoils depend on boundary-layer transition.

The second objective is to understand the behavior of boundary-layer trips in rain. In order to extrapolate wind-tunnel measurements to flight conditions, boundary-layer trips are often used on wings to increase the effective Reynolds number. The trip device fixes the location of laminar-to-turbulent boundary-layer transition, and then wind-tunnel tests are run at lower Reynolds numbers. The effect of rain on laminar-to-turbulence transition caused by boundary-layer trips on wind-tunnel models is uncertain: results are obtained here with natural, wire-, and grit-tripped transition strips on wings operated under both wet and dry conditions.

The following section describes the present wing configuration, its arrangement in the Rensselaer 4 × 6 ft wind tunnel, and the water spray system. It is followed by a presentation of measured results from surface-flow visualization and wind-tunnel-balance measurements obtained with clean, wire-, and grit-tripped wings under dry and rainy conditions. Measurements of lift, drag, and moment follow this and are correlated with these visualizations of surface water flow patterns over the wing with and without trips. The next, penultimate section discusses the flow of surface water and its relationship to the degradation of airfoil performance, and this article ends with a summary of salient conclusions.

Flow Configuration and Instrumentation

Figure 1 shows the wing section of the present study with a NACA 4412 airfoil profile, rectangular platform, 6-in. chord,

Received Dec. 30, 1994; revision received March 10, 1995; accepted for publication March 11, 1995.

*Associate Professor, Department of Mechanical Engineering, Aeronautical Engineering and Mechanics. Senior Member AIAA.
†Doctoral Student, Department of Mechanical Engineering, Aeronautical Engineering and Mechanics.
‡Masters Student, Department of Mechanical Engineering, Aeronautical Engineering and Mechanics; currently VRC Corporation, 4501 Ford Avenue, Suite 230, Alexandria, VA 22302. Member AIAA.

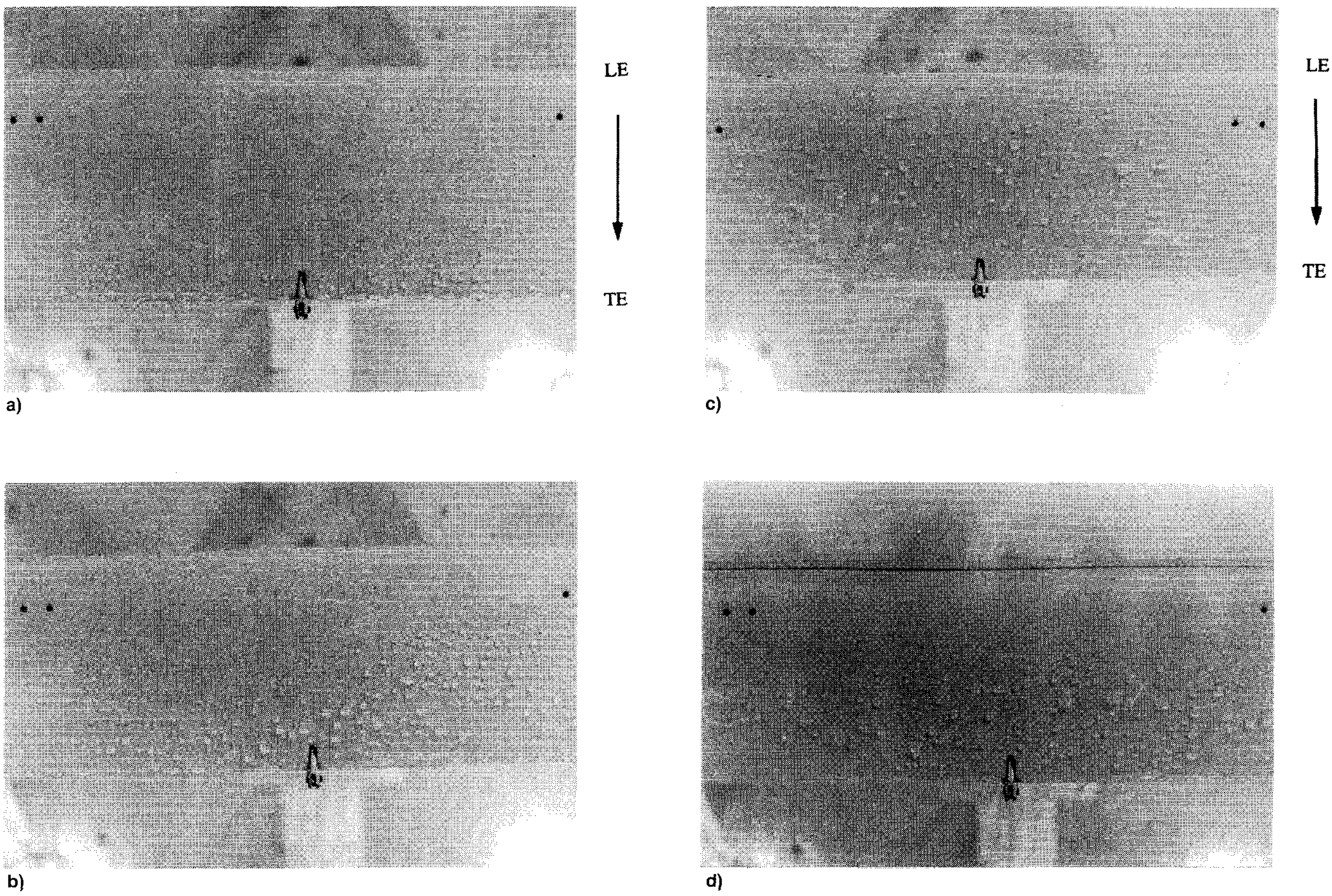

Fig. 1 Surface-water flow patterns on the suction-side of a wing: a) clean wing at 2-deg incidence, b) clean wing at 8-deg incidence, c) clean wing at 18-deg incidence, and d) wire-tripped wing at 8-deg incidence. (LE = leading edge and TE = trailing edge.)

and a span-to-chord AR of 6. The wing model was mounted in the center of the tunnel on three pressure-side struts that were supported by a six-component strain-gauge balance that allowed the measurement of force coefficients and the adjustment of wing incidence. The wingtips were square in vertical and streamwise directions and were located about 18 in. from the wind-tunnel wall so that the wing flow did not interact with the wind-tunnel boundary layers. Windows in the wind-tunnel sidewalls and roof allowed visualization of the wing surface and of the spray that was distributed uniformly in the spanwise direction over the wing, as discussed next.

Instrumentation

An external, six-component, strain-gauge balance was used to obtain mean values of aerodynamic forces and moments. Load cells were connected to amplifier circuits and then to a microprocessor-controlled data-acquisition system. Measured loads were obtained by the data-acquisition system and converted into aerodynamic forces and moments with a calibration matrix that corrected for model weight and for load-cell interactions. Angle of attack was adjusted and measured with an electronic inclinometer and then recorded by the data-acquisition system. Maximum uncertainties in lift, drag, and moment coefficients are 0.001, 0.0003, and 0.0008, respectively.

Wind-Tunnel Configuration

The Rensselaer closed-circuit, subsonic wind tunnel with a $4 \times 6 \times 20$ ft test section was operated at a static pressure of about atmospheric, at a maximum dynamic pressure of about 40 psf, at a maximum speed of about 205 ft/s (140 mph), and at a freestream turbulence factor of less than 1.06. For the present experiment, tunnel flow rate was adjusted to give a chord Reynolds number of 2.5×10^5, based on measured values of dynamic pressure obtained with a pitot tube mounted at the inlet to the test section.

To be able to spray in this tunnel, drains were added to remove up to 0.5 gpm of water accumulation, and the propeller motor that is located inside the return duct was covered with a waterproof cowling and cooled by a 300-scfm centrifugal blower. Cooling was needed to keep the enclosed motor below its recommended continuous operating temperature of 122°F. Thermocouples were located on the inductor casing and on the strut just aft of the propeller, and they continuously monitored the motor temperature that was below 110°F during full-power operation. Another advantage of this blower is that it pressurized the cowling to about 3 psi above freestream, which generated leakage flow that prevented droplets from entering the motor housing through any cracks or gaps.

Water Spray System

Figure 2 shows the spray system that produced a uniform cloud of water droplets using spray nozzles that are similar to the NASA Lewis standard icing spray nozzle and were manufactured based on the recommendations of Marek.[7] Air at 140 psi and water at pressures and flow rates up to 80 psi and 9 USGPM, respectively, were provided to the three nozzles. Bourdon-tube gauges monitored air and water pressures, and valves regulated and maintained flow rates to sustain the rain rates and droplet size that are specified later.

Preliminary experiments found that three nozzles covered the 36-in. wingspan with uniform droplet flow, and these three nozzles were mounted on a spray bar located in the plane of the wind-tunnel screens about 25 wing chords upstream of the contraction and test section as shown in Fig. 2. The bar was located about 12 in. above the airfoil centerline and adjusted

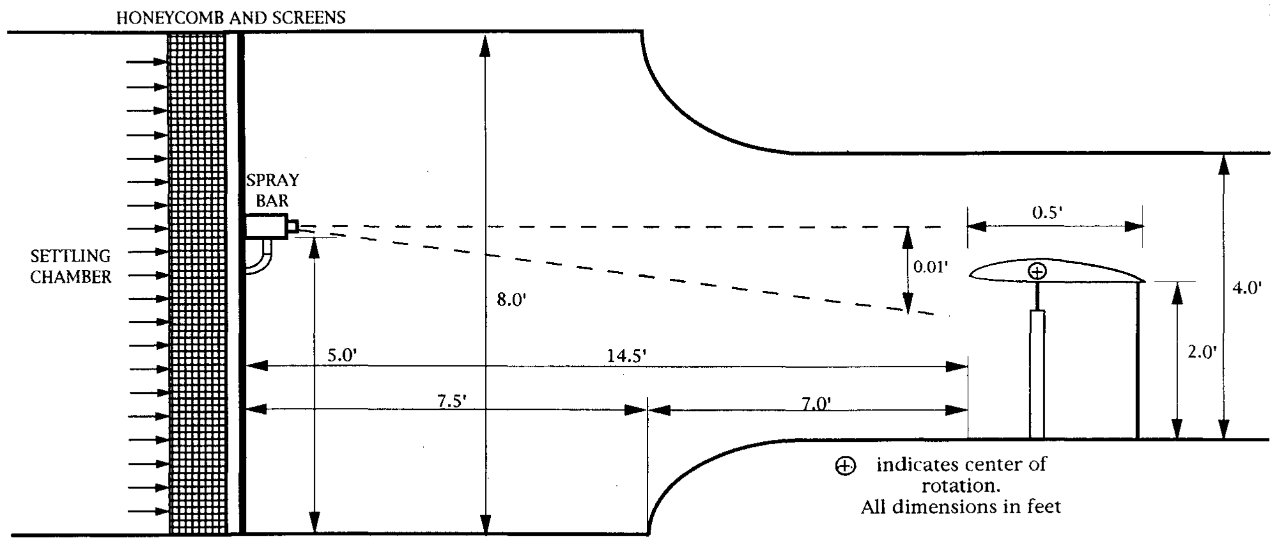

Fig. 2 Test section and spray configuration.

in the vertical direction to center the spray around the leading edge of the wing. For the results presented later, measurement in spray was performed only after the tunnel and sprayer were operated continuously and until the humidity of the tunnel was measured with an electronic hygrometer to exceed 95% relative humidity and remained stable within 1%.

Boundary-Layer Trip Devices

Transition fixing may increase the effective Reynolds number of wind-tunnel results and can be accomplished typically with the use of boundary-layer trips such as wires, tape strips, grooves, steps, or grit. These devices on the present wing would locate transition close to the trip, either because a laminar-separation, turbulent-reattachment bubble[8] occurs downstream of the trip, or because boundary layers in the low Reynolds number flow regime are extremely receptive to small disturbances.[9] Two types of transition strips were used here: a grit–trip was made from carpenter sandpaper with a uniform streamwise length of 0.25 in. and a mean grit roughness height of 0.024 in.; and a wire–trip was made by gluing a hypodermic stainless steel tube with an o.d. of 0.024 in. onto the airfoil surface. Both trips were placed on the suction side of the wing at an x/c of 0.025, which corresponds approximately to the location of peak suction pressure.

Measured Results

Figure 1a shows water sheeting at an angle of attack of 2 deg, which extends downstream to about 50% of the chord where the initial stages of rivulet formation are apparent and small beads form. Figure 1b shows water sheeting at 8-deg incidence, which ends at about 20% of the chord and the rivulets seem to have larger beads. Spanwise flow is evident at the trailing edge. Figure 1c shows evidence of large components of spanwise velocity at 18-deg incidence and water beads are stagnated in the water sheeting and rivulet formation regimes. Some reverse flow is apparent near the trailing edge at all incidences from about 2 deg less than that for maximum lift.

Figures 3–5 present increments in lift, drag, and moment coefficients, respectively, for clean (untripped), grit-, and wire-tripped wings in light-to-moderate rain. These increments are the difference between the measured values of force coefficients in rain minus that with the airfoil dry and at the same incidence. Results are presented at angles of attack from -2 deg through stall and for rainfall rates of 77–137 mm/h. All results were obtained at a chord Reynolds number of 2.5×10^5 with a mean droplet size of 18 μm and a standard deviation in droplet diameter of about 1 μm.

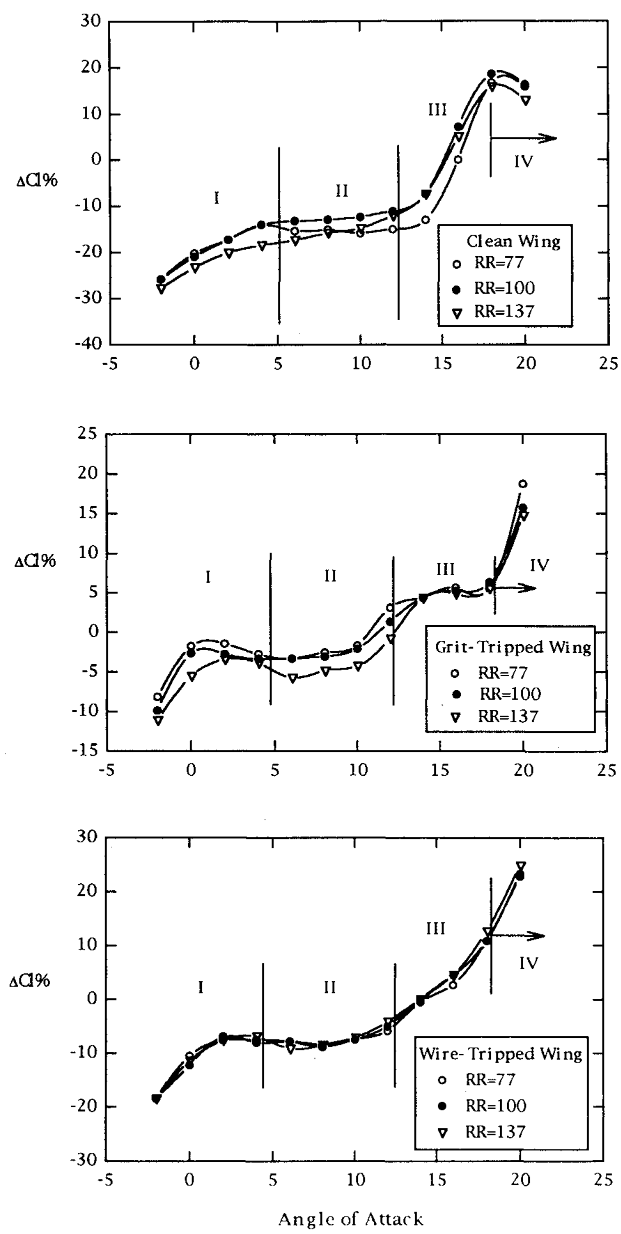

Fig. 3 Lift coefficient increments for the wing (RR = rainfall rate, mm/h).

Clean Wing

Figure 3 shows measured values of the percent change in lift coefficients that are independent of rain rate between 77–137 mm/h for the clean wing. Lift loss is constant at about 15% of lift in the range 5–12-deg incidence. At a higher incidence above maximum lift, separated flow is well developed in the surface-water flow patterns and the lift increment changes from negative to positive, which suggests the surface water is delaying separation. On an aircraft, this implies that such a wing at high incidence in rain would have a higher lift, and thus, a larger safety margin than if this wing were dry and approaching stall. Further, the lift change is more gradual, which implies that the stall would be less pronounced and controls of the aircraft would likely be more mushy than normal.

Figure 4 shows drag is increased at all incidences on clean wings. Below a 5-deg incidence, the increment in drag is constant at about 0.010, which corresponds to about a 15% increase over the dry wing. In the region of constant lift loss between 5–12-deg incidence, drag increases almost linearly with incidence and also increases with increasing rain rate. This is the only evidence in lift, drag, or moment coefficients with either clean and tripped wings of a dependence on rain rate for the range of rain rates between 77–137 mm/h reported

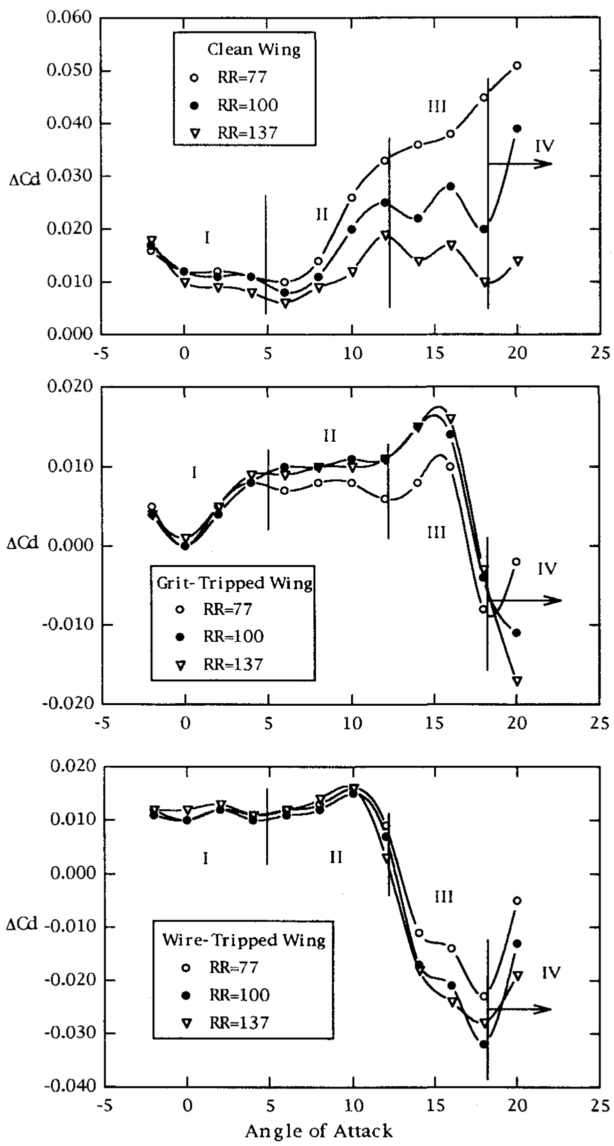

Fig. 4 Drag coefficient increments for the wing (RR = rainfall rate, mm/h).

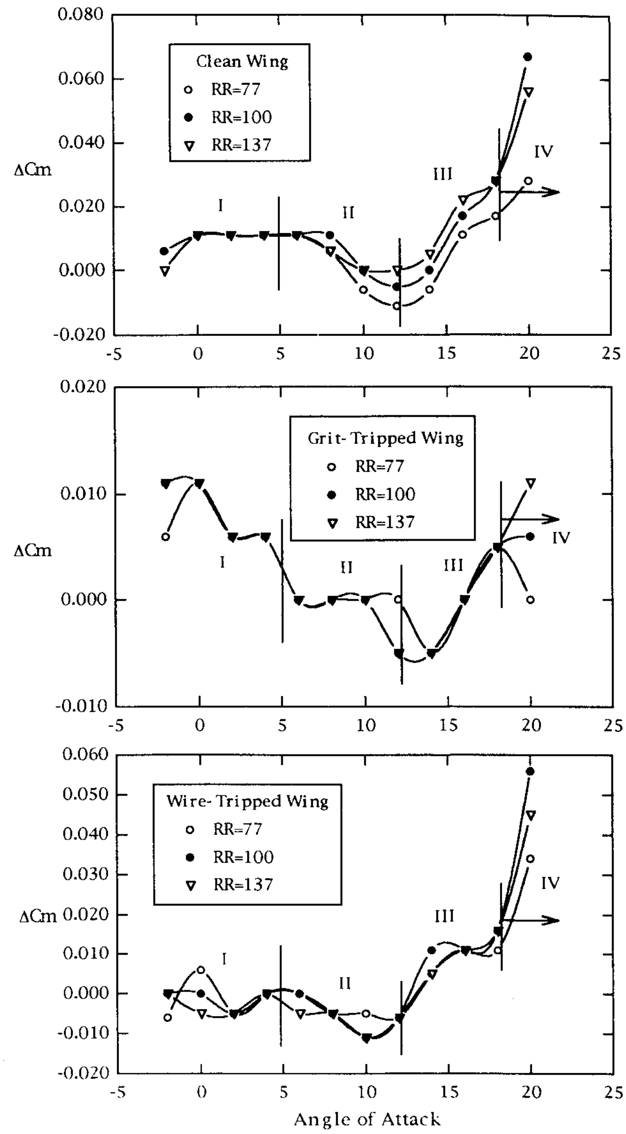

Fig. 5 Moment coefficient increments for the wing (RR = rainfall rate, mm/h).

here. Since Fig. 4 also shows that lift and moment are unaffected, it seems this linear increase in drag is associated with increased skin friction. This is supported with the flow visualization results, which suggests that the surface-water flow is becoming more turbulent with increasing incidence. At angles of attack above $C_{l_{max}}$, the drag increase is constant, although its value increased by 0.0280 when the rain rate increased from 77 to 137 mm/h.

Figure 5 shows measured values of increments in pitching moment that are again independent of the rain rate in the range investigated here. From zero incidence to maximum lift, the change in moment coefficient is negligible. Beyond the maximum lift coefficient, moment coefficient increases linearly with incidence, which suggests the application of greater than normal elevator control forces would be required to avoid stall.

Grit-Tripped Wing

The effects of rain are significantly different from the untripped wing. Figures 3–5 show that increments in lift, drag, and moment coefficient are less than half of those for the untripped wing. Lift is down by about 5% from zero to maximum lift and then about 5% above that for the clean wing from this maximum lift to stall. Drag does not show a dependence on rain rate and remains almost constant at 0.0080 for incidence below maximum lift. Approaching stall, the drag change due to rain decreases with increasing incidence and this suggests that larger turbulence in the water sheet, probably generated by the grit, is transporting momentum to the near-wall flow and this shifts the recirculation region aft, which is confirmed with flow visualization. Also, the increment in moment coefficient increases between maximum lift and stall and suggests a decrease in aft loading on the wing, which is further evidence of the separated-flow region reducing in size.

Wire-Tripped Wing

Figure 1d shows flow patterns with the wire trip for an 8-deg incidence and a rain rate of 137 mm/h. This is similar to that of the untripped wing with two notable exceptions: the bead size and extent of water accumulation at the trailing edge are larger for the wire-tripped wing. The water-sheeting region also increases in length with the wire trip and at 10-deg incidence extends downstream to about 40% of the chord before rivulet formulation is apparent.

Increments in lift, drag, and moment coefficient shown on Figs. 3–5 are again smaller than those of the clean airfoil, but are larger than those with the sandpaper trips. Measured values of lift show that the maximum lift coefficient has decreased by about 6%, with increases in rain rate from 77 to 137 mm/h and that angle of attack at maximum lift has increases from 12 to 14 deg. The distribution of lift change resembles that for the clean wing except that the decrements are about 60% smaller. Near stall, the increment in lift coefficient is larger, which is likely associated with an observed accumulation of water immediately downstream of the trip wire. The distribution of drag increment, however, resembles that for the grit-tripped wing. A constant drag increase of about 0.012 is measured below $C_{l_{max}}$ and at higher incidence drag decreases with increasing angle of attack. It is reasonable that the change in moment coefficient is negligible up to maximum lift, then behaves in a similar manner to the clean wing as did the lift increment.

Discussion

Turbulent, trailing-edge separation[8] occurs on a NACA 4412 airfoil in dry flow.[10] Measured results at high Reynolds numbers[11] suggest that laminar–turbulent transition takes place very close to the leading edge upstream of the location of pressure peak[9] and is caused by processes that occur inside the laminar boundary layer as described by Mayle.[12] At lower Reynolds numbers below 5.0×10^5, the transition process is more sensitive to freestream disturbances, aberrations of the airfoil geometry,[9] surface roughness, and Reynolds number.[13] This suggests the transition process is dominated by instabilities that originate from the inflection point in velocity above the leading-edge separation bubble,[8] which occurs on this and many other airfoils in the low Reynolds number regime.[9] Rain and the associated accumulation of surface water affect transition and cause premature laminar-to-turbulent transition of the boundary layer.

Surface Water Flow Regions

Figure 1 shows the patterns of surface flow on the upper surface of the wing for a rain rate of 137 mm/h. The painted surface of the leading edge of the entire wing is completely wetted at this rain rate. Figure 6 shows four regions with different patterns of surface flow that can be identified as follows: 1) droplet-impact, 2) film-convection, 3) rivulet-formation and 4) droplet-convection regions.

Droplet-Impact Region

The droplet-impact region[14] is observed on the present wing and is characterized by the impact of droplets both on the surface and in the growing film of surface water. It extends from the leading edge downstream to about x/c of 0.06 on the airfoils suction side for all of the rain rates and trip configurations tested here. Large craters and waves are observed in the surface film in this region. Some fog appears close to the surface, which suggests the scattering of smaller droplets back into the boundary-layer flow. This cloud of droplets may be ejecta-fog,[15] which would act to drain energy from the boundary layer as these droplets are accelerated by the local boundary-layer flow. This loss of energy affects downstream development of the boundary layer, resulting in a loss of lift and can be contributed to early flow separation[15]: this explanation is consistent with the measured loss in lift at incidence up to the separation, discussed earlier.

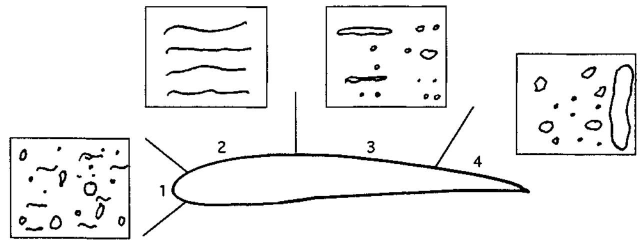

Fig. 6 Characteristics of surface-water flow regions: 1, droplet-impact region; 2, film-convection region; 3, rivulet-formation region; and 4, droplet-convection region.

Film-Convection Region

The next region downstream is the film-convection region, which is characterized by convection of a film of surface water that covers the airfoil surface like a transparent sheet. Here, surface water is dragged downstream by friction with the boundary-layer flow and appears to convect in a smooth laminar film with some surface waves and can then become turbulent. The most pronounced effect of turbulence observed in the water film was to shift the location of mean-streamline detachment aft with associated reductions in lift loss and drag gain.

Rivulet-Formation Region

Further downstream in the rivulet formation region, separate rivulets and beads form. Characteristics are similar to those found in liquid film-flow down inclined surfaces.[16,17] The sinuosity, wavelength, and amplitude of the waves of the rivulet are dependent on flow rate. Also, the distance between two sliding droplets decreases with increasing water-flow rate until a point is reached where two successive droplets touch and a single straight laminar rivulet is formed, and is consistent with the results of Schmuki and Laso.[18]

Droplet-Convection Region

Last is the droplet-convection region[3] in which the meandering rivulets are no longer stable and the beads move slowly dragged by the airflow and coalescing with other beads until all the water is dragged to the trailing edge and torn away by the external flow. The transfer of momentum in this region is dominated by the flow structure at the trailing edge. For attached boundary-layer flow, shear forces are much larger than surface tension forces in the region where suction and pressure-side boundary layers are mixing, and the surface flow breaks freely into a wake spray. For separated suction-side flow, there is accumulation of surface water upstream of the trailing edge that effects an increase in effective airfoil thickness near the trailing edge, which reduces the adverse pressure gradient approaching separation, causes the location of mean streamline detachment to move aft, and results in the measured increase in lift coefficient compared to the dry airfoil as discussed next.

Aerodynamic Performance Regimes

Results from flow visualization and force-coefficient measurement can be combined to identify the regimes I–IV shown in Figs. 3–5, each with a different flow pattern. Each regime can be defined by the extent of the droplet-impact, film-convection, rivulet-formation, and droplet-convection regions, which is correlated with measured $\Delta C_{l\%}$ values.

In regime I, the first two of the flow regions discussed earlier are observed. The first is the droplet-impact region where the water film is thick and extends back to about 5–10% of the chord. For all angles of attack, the length and nature of the droplet-impact region remained constant. The second is the film-convection region and is defined as the region with a film sheet. It extends from about 10% back to about 80% of the chord. In regime I for the incidence range from −5 to 5 deg, the lift increment shown on Fig. 3 increases almost linearly. The film-convection region decreases as the upstream boundary of the rivulet-formation region, which is characterized by beading and rivulet formulation, decreases from about 80 to 50% of the chord as the incidence increases from 2 to 5 deg. In this range the lift increment increases almost linearly with incidence as a result of a larger rivulet-formation region.

In regime II between about 5–12-deg incidence, the length of the film-convection and rivulet-formation regions remains constant. The lift increment shown in Fig. 3 also remains almost constant in this incidence range. Beads in the rivulet-formation region are about 5 mm in diameter and start some water accumulation near the trailing edge in the droplet-convection region.

In regime III between 12–18-deg incidence, the length of film-convection region again decreases. Lift increment again increases almost linearly. Figure 1c shows the film-convection region extending only to about 20% of the chord and the large beads of diameters about 10–15 mm are stagnated in the rivulet-formation and droplet-convection regions.

In regime IV at incidence above 18 deg, three-dimensional water-flow patterns are apparent over most of the wing and the lift increment remains constant with increasing incidence. In this flow regime the classic definitions of impingement, film-convection, and rivulet-formation are not applicable.

Conclusions

Experimental results are presented to quantify increments in lift, drag, and moment coefficients due to moderate rain on a wing of AR 6. These results are correlated with qualitative visualization of surface water behavior over the wing. Four flow regions are identified: 1) droplet-impingement, 2) film-convection, 3) rivulet-formation, and 4) droplet-convection regions. The percentage of the wing covered by these different flow patterns depends mainly on the angle of attack and correlates with changes in aerodynamic coefficients. Differences between the behaviors of clean, grit-, and wire-tripped wings suggest that transition fixing for wings in rain does not represent an effective increase in chord Reynolds number, and therefore, would not result in an improved correlation between flight and wind-tunnel data in moderate rain conditions.

References

[1]Landsberg, B., "1992 Accident Trends and Factors, Joseph T. Nall General Aviation Safety Report," AOPA Air Safety Foundation, Frederick, MD, 1993, pp. 3–6.

[2]Haines, P. A., and Luers, J. K., "Aerodynamic Penalties of Heavy Rain on a Landing Aircraft," *Journal of Aircraft*, Vol. 20, No. 2, 1983, pp. 111–119.

[3]Hansman, R. J., Jr., and Barsotti, M. F., "Surface Wetting Effects on a Laminar Flow Airfoil in Simulated Heavy Rain," *Journal of Aircraft*, Vol. 22, No. 12, 1985, pp. 1049–1055.

[4]Bezos, G. M., Dunham, R. E., Jr., Gentry, G. L., Jr., and Melson, W. E., Jr., "Wind Tunnel Aerodynamic Characteristics of a Transport-Type Airfoil in a Simulated Heavy Rain Environment," NASA TP 3184, April 1992.

[5]Marchman, J. F., III, Robertson, E. A., and Emsley, H. T., "Rain Effects at Low Reynolds Number," *Journal of Aircraft*, Vol. 24, No. 9, 1987, pp. 638–644.

[6]Ligrani, P. M., "Structure of Turbulent Boundary Layers, Aerodynamics and Compressible Flows," *Encyclopedia of Fluid Mechanics*, Vol. 8, 1989, pp. 111–189.

[7]Marek, C. J., "Transition Limits for Water-Droplet Crystallization with the NASA Lewis Icing Nozzle," *Journal of Aircraft*, Vol. 26, No. 9, 1989, pp. 887, 888.

[8]Chang, P. K., "Separation of Flow," 1st ed., Pergamon, New York, 1970, pp. 11–18.

[9]Mueller, T. J., "Low Reynolds Number Vehicles," AGARDograph 288, Jan. 1985.

[10]Coles, D., and Wadcock, A. J., "Flying-Hot-Wire Study of Flow Past an NACA 4412 Airfoil at Maximum Lift," *AIAA Journal*, Vol. 17, No. 4, 1979, pp. 321–329.

[11]Pinkerton, R. M., "The Variation with Reynolds Number of Pressure Distribution over an Airfoil Section," NACA Rept. 613, July 1938.

[12]Mayle, R. E., "The Role of Laminar-Turbulent Transition in Gas-Turbine Engines," *Journal of Turbomachinery*, Vol. 113, No. 2, 1991, pp. 509–537.

[13]Huber, A. F., II, and Mueller, T. J., "The Effect of Grit Roughness on the Performance of the Wortmann FX63-137 Airfoil at a Chord Reynolds Number of 100,000," Dept. of Aerospace and Mechanical Engineering, Univ. of Notre Dame, Southbend, IN, 1989.

[14]Al-Khalil, K. M., Keith, T. G., Jr., and De Witt, K. J., "Development of an Anti-Icing Runback Model," AIAA Paper 90-0759, Jan. 1990.

[15]Bilanin, A. J., "Scaling Laws for Testing High Lift Airfoils Under Heavy Rain," AIAA Paper 85-0260, Jan. 1985.

[16]Towell, G. D., and Rothfeld, L. B., "Hydrodynamics of Rivulet Flow," *AIChE Journal*, Vol. 12, No. 5, 1966, pp. 972–980.

[17]Nakagawa, T., and Scott, J. C., "Stream Meanders on a Smooth Hydrophobic Surface," *Journal of Fluid Mechanics*, Vol. 149, No. 1, 1984, pp. 89–99.

[18]Schmuki, P., and Laso, M., "On the Stability of Rivulet Flow," *Journal of Fluid Mechanics*, Vol. 215, No. 1, 1990, pp. 125–143.